Bioprocess Biosyst Eng
DOI 10.1007/s00449-015-1408-5

ORIGINAL PAPER

Nano-CeO_2 decorated graphene based chitosan nanocomposites as enzymatic biosensing platform: fabrication and cellular biocompatibility assessment

Sriparna De[1] · Smita Mohanty[1,2] · Sanjay Kumar Nayak[1,2]

Received: 7 January 2015 / Accepted: 22 April 2015

Abstract The present study summarizes the designing of a green transducer phase based on nano-cerium oxide (CeO_2) decorated reduced graphene oxide (RGO) reinforced chitosan nanocomposites as an effective enzyme immobilizer and bio-sensing matrix for glucose analyte. Also, it scrutinizes the biocompatibility and cell viability of the synthesized nanohybrid with human fibroblastic macrophage cell line. CeO_2 nanoparticles (NPs) were successfully grown on graphene nanosheet in the presence of cationic surfactant followed by facile hydrothermal treatment. The eventual growth of synthesized CeO_2 nanocrystals on the graphene layer was confirmed from X-ray diffraction (XRD), transmission electron microscopy (TEM) and Raman analysis. The biocompatibility of the synthesized nanohybrid was also evident from the MTT assay. Glucose oxidase (GOx) was employed on the green polymer nanocomposites modified FTO electrode to fabricate an enzymatic bioelectrode. The electroanalytical response of the GOx/nano-CeO_2/RGO/CS/FTO bioelectrode towards electrooxidation of glucose analyte was investigated by electrochemical impedance (EIS) and cyclic voltammetry (CV) study. The resulting biosensor exhibited a good electrochemical response to glucose within the linear detection range of 0.05–6.5 mM with a low detection limit of 2 μM and a sensitivity of 7.198 μA mM^{-1} cm^{-2}. The bioelectrode also showed good shelf life ($\sim$10 weeks) and negligible interfering ability under controlled environment. The obtained results indicate that nano-CeO_2/RGO nanohybrid based chitosan nanocomposites achieve a biocompatible biosensing platform for effective enzyme immobilization due to the excellent synergistic effects between the CeO_2 nanoparticles and graphene sheet.

Graphical abstract

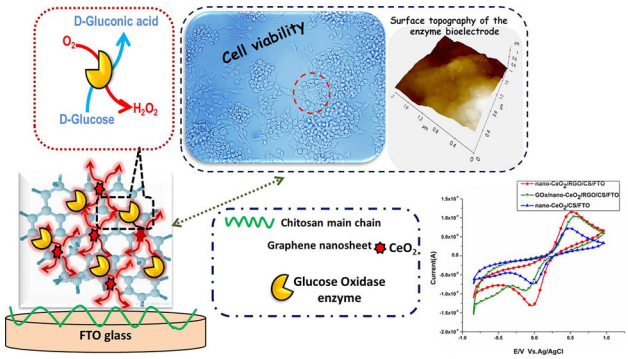

Keywords Green material · Graphene · CeO_2 nanoparticles · Nanohybrid · Enzyme immobilization · Biocompatibility

Introduction

In the last few decades, the strategy of designing an effective biosensing transducer podium based on various functional polymeric nanocomposites hold great potential to provide an early detection of various metabolic body disorders and diseases [1]. The implementation of a new diagnostic tool, implantable electrochemical biosensor from naturally occurring biopolymers-based green

✉ Smita Mohanty
papers.journal@gmail.com

[1] Central Institute of Plastics Engineering and Technology (CIPET), Chennai, India

[2] Laboratory for Advanced Research in Polymeric Materials (LARPM), CIPET, Bhubaneswar 751 024, Odisha, India

Published online: 17 May 2015

nanocomposites has received an utmost scientific recognition to scrutinize such serious metabolic disorder like diabetes and obesity [2]. Among them diabetes mellitus have been found to be a worldwide epidemic which is a leading cause of mortality and several complications for human health, such as diabetic retinopathy, neuropathy, nephropathy, pulmonary dysfunction, and as well as some coronary heart diseases [3]. In realization, glucose biosensor research in diabetes management has recently gained a considerable attention and it has been most intensely investigated by fabricating a reliable bioelectronic sensing device for glucose detection, with excellent execution to achieve good response time, improved sensitivity, better biocompatibility, transducer phase suitability among the other enzyme biosensors [4, 5].

Recently graphene and graphene-based nanohybrids have been appreciated for widespread application in several research areas including electronics [6], Li-ion batteries [7], fuel cells [8], supercapacitors [9], sensors [10], and biosensors [11] due to its fascinating properties such as high electrical conductivity and thermal conductivity, large specific surface area, superb charge-carrying capacity and definite flexibility [12–14]. Systematic distribution of metal oxide NPs such as ZnO, TiO_2, Co_3O_4, ZrO_2, SnO_2 on the graphene layer evolves a nanohybrid with large electroactive surface area and enhanced charge transfer network, promoting it a suitable matrix for the fabrication of transducer phase in biosensing device [15–22]. Among them, CeO_2 is one of the most prominent earth materials, which has attracted considerable attention for various applications owing to its high chemical stability, high oxygen storage capacity, huge electroactive surface [23, 24]. The major area of applications includes environmental science, catalysis, fuel cells, solar cells, and biosensing array [25]. However, in solution phase, graphene based nanohybrid, possess the tendency to form agglomerated clusters, which could restrict the entrapment and bioactivity of the GOx enzyme [26]. The lacuna has been well addressed through reinforcing or incorporating these nanohybrids within relevant polymers specially biopolymers [27] which generates a suitable microenvironment for enzyme immobilization. Further, these composed green electrode material with better efficacy are also said to be biocompatible and non-toxic that fulfill the demand of maturation of transducer phase in biosensing device. Chitosan, is a naturally abundant cationic biopolymer that has drawn considerable attention in the fabrication of the biosensing platform because of its excellent film-forming ability, functionality, and biocompatibility make it a promising candidate for immobilization of bioactive molecules such as enzymes [28]. In combination with graphene nanohybrids, chitosan nanocomposites render a potential transducer platform to construct an enzymatic biosensor.

Many graphene-based nanohybrid systems have been reported as a template for the transducer phase of sensing device to electrochemically detect glucose [29, 30], NADPH [31], cytochrome c [32], neurohormone dopamine [33, 34], and organophosphate pesticides (OPs), [35] etc. Several biosensing platforms have been already identified such as graphene/Cu nanoparticles [36], graphene/Pd [37], reduced graphene oxide (RGO)-multiwalled carbon nanotube (MWCNTs) [11], and RGO/ZnO [38]. Moreover, Li et al. synthesized CeO_2-loaded graphene nanocomposites with high specific capacitance and power density [39]. In addition Bai et al. [40] also introduced a simple route to prepare CeO_2/graphene nanocomposite for efficient anode material of lithium ion batteries. Very recently, Mahmoud et al. fabricated gold-decorated graphene nanohybrid and investigated its efficiency in glucose biosensing [41].

A facile route to harness the excellent properties of chitosan, graphene, and CeO_2 NPs for transducer phase in glucose sensing applications is by integrating them into nanocomposite materials. In this present work an attempt has been undertaken toward the fabrication of nano-CeO_2/RGO nanohybrid reinforced chitosan (CS) nanocomposite matrix as an efficient biosensing platform in biosensor device. Further, GOx enzyme has been effectively immobilized onto the chitosan nanocomposite matrix and investigated through topographical analysis. The electrochemical performance of the fabricated enzyme bioelectrode was studied in detail using electrochemical impedance spectroscopy (EIS), cyclic voltammetry (CV), and differential pulse voltammetry (DPV). The fabricated bioelectrode revealed high sensitivity, low detection limit, and acceptable glucose detection range. The biocompatibility of the nanohybrid was also assessed through MTT assay, which is highly required for the development of transducer phase in biosensing device.

Experimental details

Materials

Graphite flakes (45 μm), chitosan (viscosity average mol. wt-190,000-310,000, DD 75–85 %), and glucose oxidase (GOx) from *Aspergillus niger* (EC 1.1.3.4, Type X, 100,000–250,000 units/g, lyophilized powder) have been purchased from M/s Sigma-Aldrich (USA). Ceric ammonium nitrate (99 % pure) and D-glucose have been procured from M/s TCI chemical Pvt. Ltd. (Chennai, India) and M/s Sisco Research Laboratory Pvt. Ltd. (Mumbai, India), respectively. Phosphate buffer saline (PBS 50 mM, pH 7.2) with 0.1 (M) KCl was used as a supporting electrolyte. The stock GOx solution was freshly prepared in PBS buffer, and stored at 4 °C when not in use. A solution of D-(+)

glucose was also prepared and kept for 24 h to mutarotate at room temperature.

For electrode fabrication, fluorine-doped tin oxide (FTO) glass plate (25 mm × 25 mm × 1.1 mm) of surface resistivity ~15 ohm sq.$^{-1}$ was purchased from M/s Shilpa Enterprises (Nagpur, India). The working surface area has been assigned as 0.25 cm^2. All other chemicals and reagents like potassium permanganate ($KMnO_4$), cetyltrimethylammonium bromide (CTAB), conc. H_2SO_4, HCl etc., were of analytical grade.

Synthesis of nano-CeO_2/RGO nanohybrid

The detailed synthesis of reduced graphene oxide (RGO)-imprinted CeO_2 nanoparticle was adopted and synthesized as per earlier described method with little modification [20]. At first, GO was synthesized from graphite flakes using hummers' method [42]. Briefly, 3 g of graphite powder was suspended in 80 ml concentrated H_2SO_4 and the solution was stirred for about 24 h in an ice water bath (0 °C). Then, 9 g of $KMnO_4$ was added slowly in stirring condition and the temperature was calibrated at 0 °C to avoid sudden increment of reaction temperature. The solution mixture was kept in stirring condition for about 1 day and then diluted gradually with 140 ml deionized water. Again, 150 ml water was poured into the solution and left for stirring of about 3 h. Thereafter, 3 % H_2O_2 was added dropwise into the solution and the significant color change from brown to yellow–brown was noticed. The resultant solution was filtered carefully and washed several times with HCl (3 %) and deionized water to neutralize the pH. Finally, the obtained product was subjected to centrifugation at 2000 rpm for 30 min repeatedly and the dark brown sediment of GO was collected and dried at 50 °C under vacuum.

In the second step, a certain amount of GO was dissolved in 50 ml of deionized water followed by ultrasonication. Then, 0.01 (M) of ceric ammonium nitrate containing CTAB surfactant (~0.10 g) was gradually poured into the above-prepared solution with vigorous magnetic stirring to form a highly dispersed solution mixture. Simultaneously, 25 % aqueous ammonia solution was added slowly and the mixture was kept under constant stirring for about ~5–6 h. The pH of the solution was adjusted to 10 and was maintained under continuous stirring. Afterward, the obtained solution (50 ml) was transferred into a Teflon-lined jar and placed in stainless steel tank to conduct the hydrothermal treatment at ~120 °C for 12 h. The resulting nano-CeO_2/RGO suspension was filtered carefully and washed several times with water. The supernatant was discarded and the final product was dried at 50 °C under vacuum followed by ultrasonication to procure a fine powder.

Fabrication of GOx/nano-CeO_2/RGO/CS/FTO nanobioelectrode

FTO electrode was successively cleaned with 1:1 chromic acid, ethanol, deionized water, and acetone and dried at ambient temperature. Initially, 0.5 % chitosan solution was prepared. Then 6 mg of pre-synthesized nano-CeO_2/RGO nanosheet was dissolved in 2 ml of 0.5 % chitosan solution. 10 µl aliquot was taken from the above-prepared colloidal solution and cast on FTO electrode and left for drying at controlled environment. The developed electrode was totally immersed in GOx suspension (2 mg ml^{-1}) dispersed in PBS buffer (50 mM, pH 7.2) for ~24 h at 4 °C to immobilize the enzyme completely. Subsequently, the assembled bioelectrode was properly rinsed with deionized water to remove any unbound GOx fragments and stored in a controlled environment. For comparison purpose other bioelectrodes were also prepared following the above derived procedure. The stepwise fabrication scheme has been illustrated in Scheme 1.

Characterization

The crystalline phase and size analysis of the synthesized products have been carried out using wide angle X-ray diffractometer (Shimadzu XRD-700L, X-Pert MPD, Japan) equipped with Cu Kα radiation ($\lambda = 0.1514$ nm). The products such as nano-CeO_2 and nano-CeO_2/RGO nanohybrid were scanned over the range of diffraction angle $2\theta = 10^{o}$–70^{o} with a scan speed of 5° min^{-1}. The surface topography of the modified electrodes has been studied using an atomic force microscope (M/s Park Scientific Instrument, XE-100, Korea) in non-contact mode and a commercial probe was used at moderate pressure and room temperature. The dimension and dispersion of the synthesized products were investigated on JEM 1400 transmission electron microscope (TEM) (JEOL, Japan) at an accelerated voltage of 80 kV. The samples were fully dispersed in ethanol followed by ultrasonication and then it was mounted on a copper TEM grid. The Raman spectra were recorded at the room temperature using Micro-Raman spectrometer (Model: inVia, M/s Renishaw Plc, UK; Sl No-H33197) over the range of 100–3500 cm^{-1}. The argon ion (Ar) laser (514 nm, 50 mW) has been used in the analysis. To measure the surface hydrophilicity, contact angle measurement was carried out using a sessile drop method of contact angle measurement on Phoenix, SEO, Korea. Deionized water was taken as liquid phase.

In vitro cellular biocompatibility assay

To check the cellular biocompatibility, mouse monocyte macrophage cell line (Raw 264.7) was used for the cell

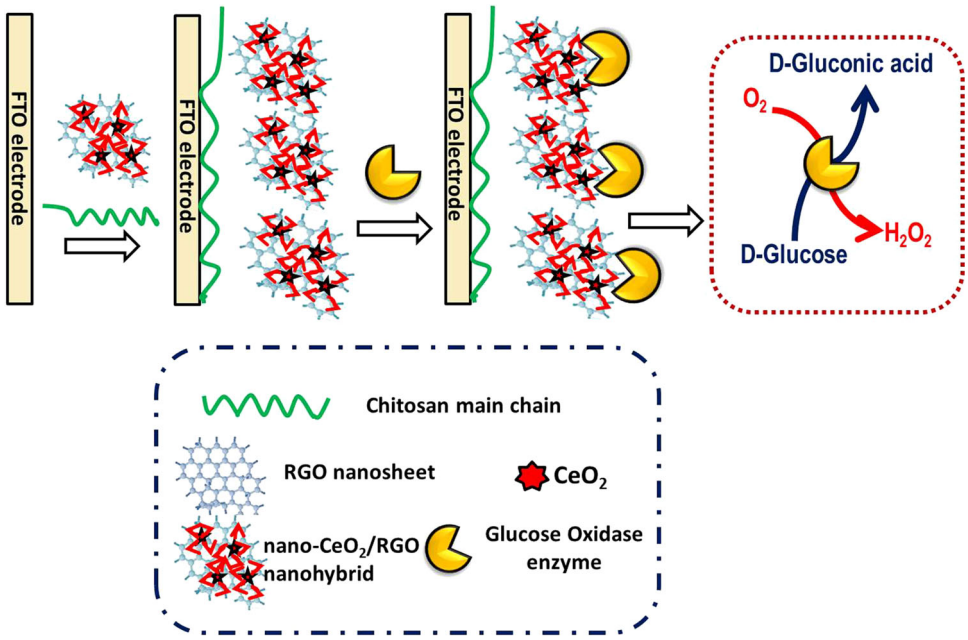

Scheme 1 Schematic illustration of the stepwise glucose biosensor fabrication

biocompatibility MTT [(3-[4,5-dimethyltriazol-2-y1]-2,5-diphenyltetrazolium] and cell proliferation assay. The cells were cultured in Dulbecco's modified Eagle's medium (DMEM, ATCC) supplemented with 10 % fetal bovine serum (FBS, ATCC) and 1 % penicillin/streptomycin (ATCC). The cell suspension was added into 25 cm^2 vials and put into an incubator (37 °C, 5 % CO_2) followed by trypsinization. Simultaneously, the cultured cells ($\sim 2 \times 10^4$ cells per well) were seeded within 96 well plate and again incubated in DMEM solution for MTT assay. Seven concentrations (500–5 μg ml^{-1}) of nano-CeO_2/RGO nanohybrid was suspended in these 96 well plates and incubated thereafter in an incubator (37 °C, 5 % CO_2) for 24 and 48 h, respectively.

Results and discussion

Characterization of the synthesized nanohybrid

X-ray diffraction analysis

Figure 1 illustrates the X-ray diffraction (XRD) patterns and the crystal plane of synthesized products. According to the XRD pattern of RGO, a new broad peak (002) appeared in the range of 17.4°–18.1° and corresponding inter-planar distance was obtained as ~0.50 nm, which is attributed to the introduction of oxygen-containing functional group and the formation of a few layers of graphene nanosheet after exfoliation. XRD spectrum of synthesized CeO_2 exhibits several characteristic peaks at 28.6° (111), 33.2° (200), 47.3° (220), 56.5° (311), 68.7° (322), and 69.9° (400).

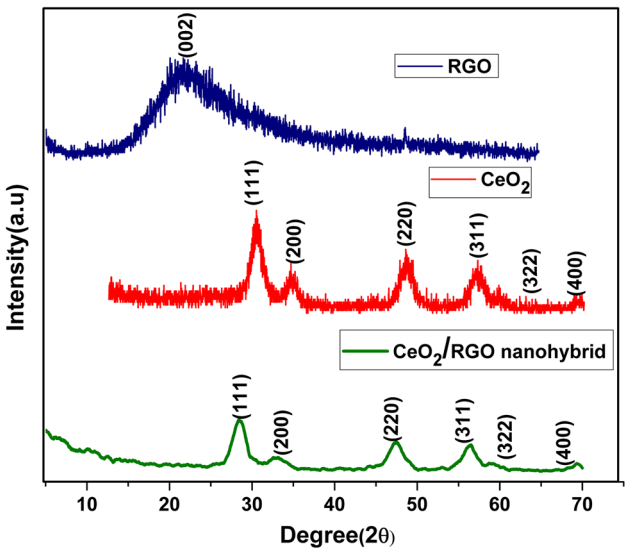

Fig. 1 X-ray diffraction pattern of CeO_2 nanoparticles, RGO, and nano-CeO_2/RGO nanohybrid

Similar diffraction pattern with minute differences in peak intensities were also noticed in case of synthesized nano-CeO_2/RGO nanohybrid. The diffraction was found to be very close proximity to that of CeO_2 nanoparticles and it was highly consistent with face-centered cubic fluorite structure of CeO_2, indicating the successful imprint of nano-CeO_2 on the layered surface of graphene nanosheet. This aspect can also be justified by the fact that hydrothermal treatment leads to the formation of uniform building blocks on RGO nanolayers which in turn facilitates the growth of CeO_2 nanoparticles. The average

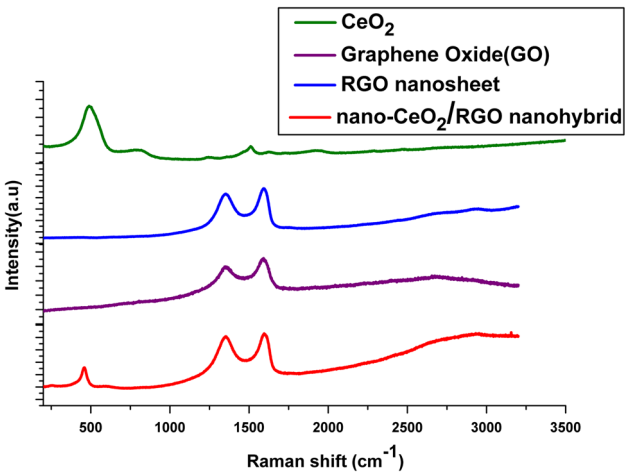

Fig. 2 Raman spectra of graphene oxide (*GO*), CeO_2 nanoparticles, RGO, and nano-CeO_2/RGO nanohybrid

crystalline domains of CeO_2 and nano-CeO_2/RGO powder was measured using the Scherrer's formula $d = 0.9\lambda/\beta \cos\theta$ where λ is the wavelength of X-ray (0.154 nm), β is the half width maximum intensity, and θ is the Bragg's angle. The average crystallite size of CeO_2 in nano-CeO_2/RGO nanohybrid was obtained as $\sim$2.5 nm which was relatively higher than the CeO_2 nanoparticles ($\sim$0.13 nm). These results are quite similar to the findings reported by other authors [43, 44].

Raman analysis

Figure 2 elucidates the Raman spectra of GO, RGO, CeO_2 NPs, and the nano-CeO_2/RGO nanohybrid. From the spectra it can be seen that two well-defined peaks appeared in the range of 1330–1592 cm^{-1}, which correspond to the *D* and *G* bands of graphene. In which *D* and *G* band signifies the *k*-point phonons of A_{1g} symmetry and E_{2g} phonon of the C sp^2 atoms, respectively [33]. The observed *D*/*G* band intensity ratio of nano-CeO_2/RGO nanohybrid ($\sim$1.01) was higher than that of GO ($\sim$0.87), whereas RGO nanosheet exhibited a *D*/*G* intensity ratio of ($\sim$0.92), indicating the minor crystal defects present in nano-CeO_2/RGO nanohybrid relative to RGO nanosheet. Furthermore, in case of nano-CeO_2/RGO nanohybrid an additional peak at $\sim$460 cm^{-1} was observed, which might be due to the F_{2g} symmetric stretching mode of the Ce–O_8 vibrational unit thus confirming the successful growth of CeO_2 NPs on the RGO nanosheet. Therefore, the obtained results are consistent enough as per previous literature [20, 44].

Morphological studies

Morphologies of various synthesized nanohybrids were investigated and characterized by TEM and AFM analyses. As displayed in Fig. 3a nano-CeO_2/RGO nanohybrid reveals the randomly dispersed hexagonal and some quasi-spherical CeO_2 NPs fabric onto the wrinkled graphene sheet which suggests a successful decoration of CeO_2 NPs onto the graphene layer. It can be seen from Fig. 3b, graphene exhibits typical folded structural arrangement with relatively creased surface texture. The average grain size of these NPs has been obtained as $\sim$7–10 nm which is quite high as calculated from XRD data, implying agglomerated CeO_2 NPs (Fig. 3c) nanoclusters.

Further, the successful decoration of CeO_2 NPs on the graphene nanosheet was also monitored by AFM analysis (Fig. 3d). It exhibits a thicker graphene nanosheet ($\sim$10 nm) which is supposed to be higher than the well-known thickness of graphene sheet ($\sim$0.34 nm). This is attributed to the presence of functionalized groups on both sides of exfoliated graphene oxide (GO) as well as marginal defect introduced by successive oxidation process. It further indicates that the successful decoration of CeO_2 NPs on the graphene nanosheet results in the increase in thickness of the nanohybrid.

In vitro cell biocompatibility assessment of nano-CeO_2/RGO nanohybrid

MTT assay was used to investigate the cell viability. It is noticed that mitochondrial enzyme present in the cell has been found to be capable of reducing MTT. The cell viability and proliferation was scrutinized at 24 and 48 h after cell seeding. From Fig. 4 it can be seen that with the decrease in nano-CeO_2/RGO nanohybrid concentration from 500 to 5 μg ml^{-1}, the in vitro cell viability numbers increased from 31.5 to 94.4 % (compared to cell control as 100 %).

As observed from Fig. 4, after 48 h incubation more than $\sim$95 % macrophage cells are alive in nano-CeO_2/RGO nanohybrid seeded culture media, indicating that the cell survival and proliferation was not restricted by the presence of nano-CeO_2/RGO nanohybrid which was ascribed to the engulfment of NPs by building a self-defense barrier toward successive growth of cells. This confirms the less toxic nature of nano-CeO_2/RGO nanohybrid, which assists the cell growth and maintains the cell viability in the culture media [45–50]. These assumptions are also supported by the microscopic images as shown in Fig. 5. The cytoplasmic condensation of macrophage cells was noticed at high concentration of nanohybrids resulting in the inhibition of cell proliferation to some extent. Furthermore, after prolonged incubation (48 h), the viable macrophage cells with irregular cell clumping caused confluent cell aggregation. However, no such effects were visible with low nanohybrid-incubated

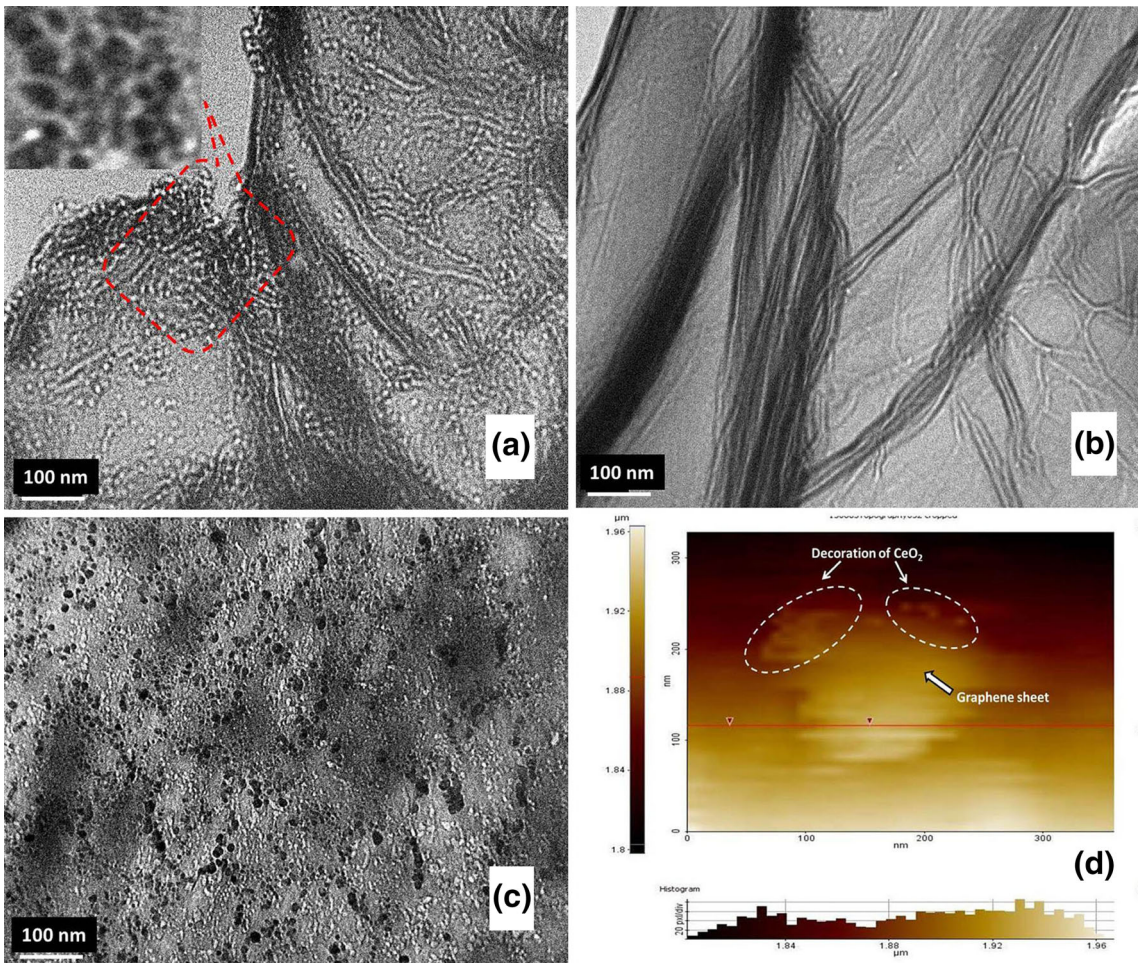

Fig. 3 TEM micrograph of **a** CeO_2-decorated RGO nanohybrid, **b** RGO, **c** CeO_2 nanoparticles, **d** AFM topography of CeO_2-decorated RGO nanohybrid

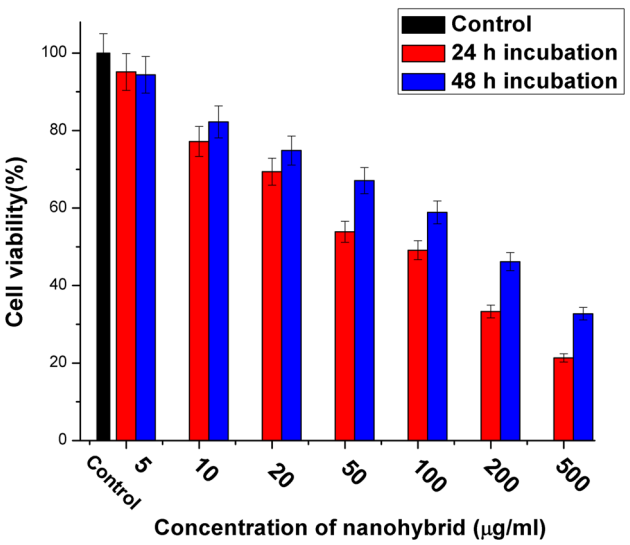

Fig. 4 Cell viability of macrophage cell *line* in MTT test cultured with different concentration of nano-CeO_2/RGO nanohybrid for 24 and 48 h

cell culture media that proves that the less toxic nano-CeO_2/RGO nanohybrid can be efficiently utilized as a biocompatible material in biosensing device.

Topographical and surface hydrophilicity studies of chitosan-based modified electrodes

To confirm the successful enzyme entrapment on the modified electrode, the AFM technique has been employed. As can be seen in Fig. 6anano-CeO_2/RGO/CS/FTO electrode reveals the porous, globular surface microstructure with mean surface roughness value (RMS) of ~100 nm. The observed value of RMS depicts the uniform distribution of nanopores and granular structure on the electrode surface, which is highly significant for biosensing array in terms of charge transportation. Moreover, CeO_2 NPs were securely distributed on the graphene layers, creating some phase separation (Fig. 6a). Conversely, GOx immobilization has led to comparatively smooth and even surface texture, resulting in the decrease of surface

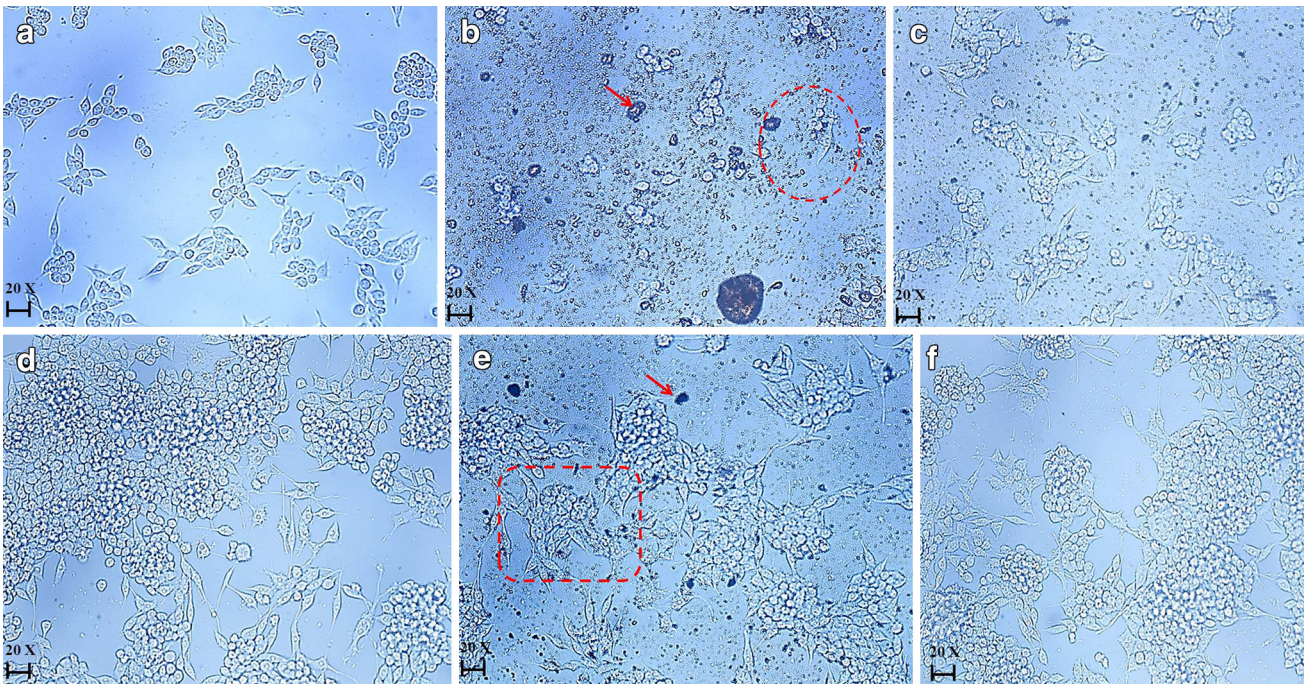

Fig. 5 Light microscopy images (×20 magnification) of cell cultures after 24 h incubation **a** control, **b** nano-CeO_2/RGO nanohybrid (500 μg ml^{-1}), and **c** nano-CeO_2/RGO nanohybrid (5 μg ml^{-1}); after 48 h incubation **d** control, **e** nano-CeO_2/RGO nanohybrid (500 μg ml^{-1}), and **f** nano-CeO_2/RGO nanohybrid (5 μg ml^{-1}). *Arrows* indicate nano-CeO_2/RGO nanohybrids, cycle and *rectangle* imply cell shrinking and irregular confluent cell aggregates, respectively

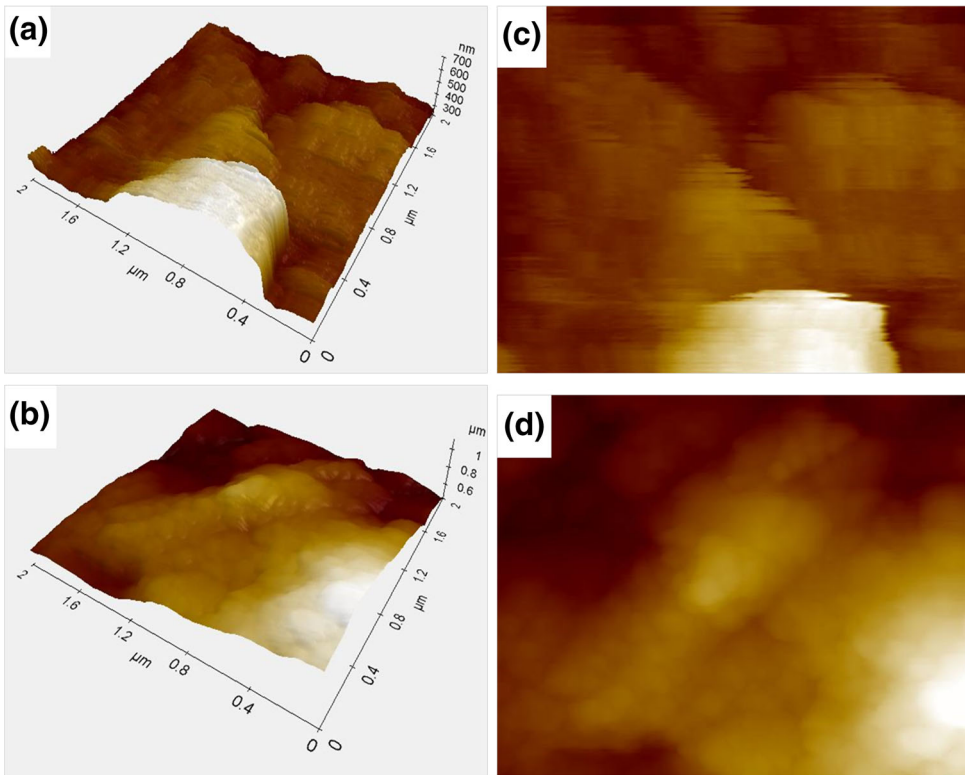

Fig. 6 3D topographic images of different FTO electrode **a** nano-CeO_2/RGO/CS/FTO, **b** GOx/nano-CeO_2/RGO/CS/FTO bioelectrode; 2D phase morphology of **c** nano-CeO_2/RGO/CS/FTO, **d** GOx/nano-CeO_2/RGO/CS/FTO bioelectrode

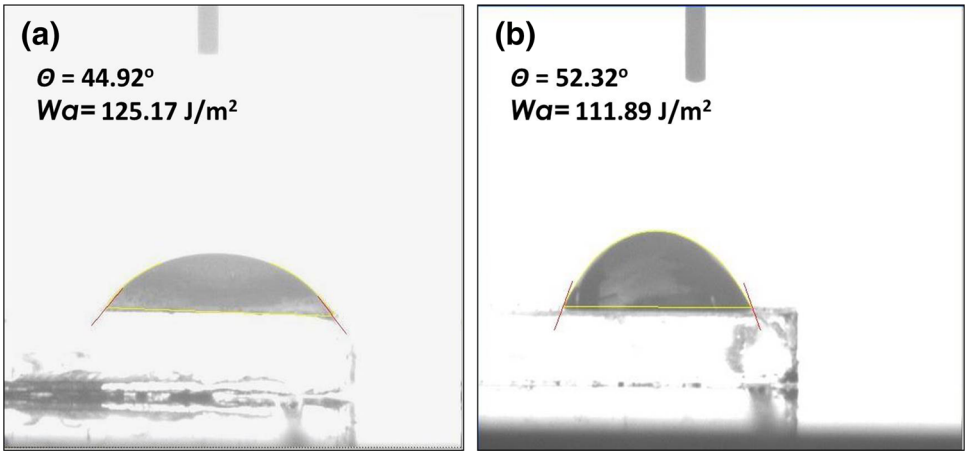

Fig. 7 Contact angle measurement of **a** nano-CeO_2/RGO/CS/FTO, **b** GOx/nano-CeO_2/RGO/CS/FTO bioelectrode

roughness value (RMS = 40.2 nm; Fig. 6b). Therefore, the appearance of dense cloudy surface topography by dissipating globular forms suggests that GOx was effectively consumed on the nano-CeO_2/RGO nanohybrids-modified chitosan layer (Fig. 6c, d). Similar observation has been also reported by the other researchers [51].

To evaluate the surface hydrophilicity contact angle (CA) measurement was carried out with the nano-CeO_2/RGO/CS/FTO and GOx/nano-CeO_2/RGO/CS/FTO bioelectrodes. The initial contact angle was derived immediately after water dropped on the electrode surface to express the wettability and surface hydrophilicity of the matrix in terms of surface tension (γ) and work of adhesion (W_a).The work of adhesion can be estimated from the Young–Dupre Eq. (1).

$$W_a = \gamma\,(1 + \cos\theta), \tag{1}$$

where θ is the contact angle between the water droplet and the modified electrode surface. The nano-CeO_2/RGO/CS/FTO electrode (Fig. 7a) shows the lowest CA value of 44.92° revealing the hydrophilic nature of nano-CeO_2/RGO nanohybrid. This assists the spreading of water droplets on the electrode surface resulting in the increase in work of adhesion value to 125.17 J m^{-2}. However the measured CA increased to 52.32° after the glucose oxidase was immobilized on the nano-CeO_2/RGO/CS/FTO electrode (Fig. 7b) surface indicating that these fabricated bioelectrode has relatively weaker affinity to the hydrophilic moiety imparting hydrophobic in nature. Additionally, the lower work of adhesion ($\sim$111.89 J m^{-2}) of the bioelectrode restricts the wettability of the hydrophilic moiety on the enzyme-linked electrode surface by reducing the surface energy to some extent. Thus, it was confirmed that, incorporation of nanohybrids forms a higher energy electrode surface which could improve the hydrophilicity as well as wettability.

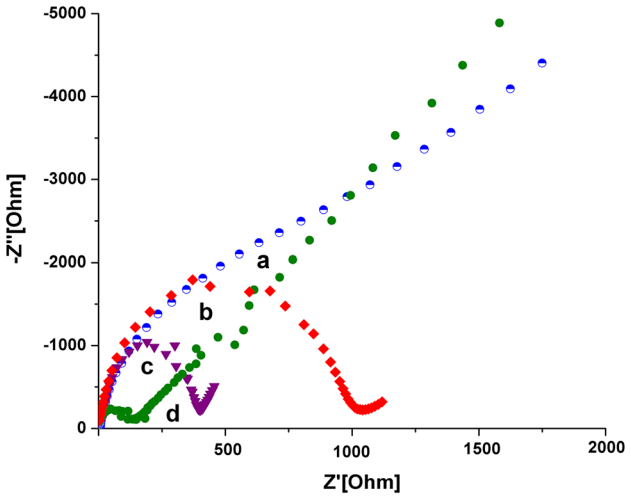

Fig. 8 Electrochemical impedance spectra of various modified electrodes

Electrochemical studies

Electrochemical impedance spectroscopy

Figure 8 shows the Nyquist plot of EIS measurement that was carried out on (a) nano-CeO_2/CS/FTO, (b) bare FTO, (c) GOx/nano-CeO_2/RGO/CS//FTO, and (d) nano-CeO_2/RGO/CS/FTO in PBS [50 mM, pH 7.2, 0.1 (M) KCl] containing 2.5 mM $[Fe(CN)6]^{3-/4-}$ within the frequency range of 0.01–10^5 Hz at initial potential of 0.1 V and amplitude of 10 mV. The Nyquist plot illustrates the semicircle diameter at higher frequency analogs to the charge transfer resistance (R_{ct}) and the linear part of lower frequency region corresponds to the diffusion-controlled process of redox probe [52–54].

The Nyquist plot noticed for bare FTO electrode exhibited a large semicircle with an electron transfer resistance

(R_{ct}) of 1085 Ω. Incorporation of CeO_2 NPs within the chitosan matrix, the R_{ct} was decreased to 810 Ω indicating an increase in the electron transfer process at modified electrode surface due to the presence of conducting CeO_2 NPs. In case of nano-CeO_2/RGO/CS/FTO electrode, the R_{ct} value was further decreased to 175 Ω which is ascribed to the fact that CeO_2 nanoparticles decorated reduced graphene oxide nanosheet facilitates the mobility of electron transfer between the redox probe of $[Fe(CN)6]^{3-/4-}$ and the electrode surface. However, immobilization of glucose oxidase (GOx) enzyme led to the increase in semicircle diameter of 387 Ω. This result can be attributed to the fact that nano-CeO_2/RGO/CS nanocomposites offer a suitable microenvironment on which GOx enzyme, was effectively assembled, resulting in obvious increment of charge transfer resistance.

Cyclic voltammetry

To evaluate the possible synergistic effects between CeO_2 NPs and RGO nanosheet, the CV response of $[Fe(CN)_6]^{3-/4-}$ at the FTO electrode surface and the other modified electrodes were recorded (Fig. 9a). For a comparative purpose, the CV analysis was also performed with these modified electrodes as controls (Fig. 9b). nano-CeO_2/RGO/CS//FTO electrode shows the distinct redox behavior at 0.51 V (E_{pa}) and its corresponding anodic peak current was obtained at 1.15×10^{-4} A. This highest value of current response was primarily due to the anchoring of cerium oxide nanoparticles on the RGO nanosheet which accelerates the tunneling of electrons that promotes increased electron transportation through the chitosan layer. Further, the significant reduction of anodic peak current response was observed in the case of CeO_2 NPs-modified electrode (7.16×10^{-5} A) which is possibly due to the fact that only CeO_2 NPs could not amplify the peak current response to a greater extent. However, the magnitude of current response for GOx-modified nano-CeO_2/RGO/CS//FTO bioelectrode decreased to 1.03×10^{-4} A, suggesting that effective immobilization of GOx on the nanobiofilm generates an insulating layer which restricts the facile electron transfer between the redox probe and the electrode surface.

Electrochemical response study

The electrochemical response of proposed fabricated bioelectrode GOx/nano-CeO_2/RGO/CS/FTO has been investigated using the amperometric DPV technique at a fixed scan rate of 50 mV s^{-1} in PBS buffer (50 mM, 0.1 (M) KCl). Figure 10a shows the typical DPV response curves with different concentration of glucose. It can be observed that a well-defined oxidation peak at 0.38 V was attributed to the redox property of CeO_2-decorated RGO nanohybrid. The result was also ascribed to the intercalation of the surfactant on the RGO nanosheet which refines the hydrophilicity of the electrode surface. Therefore, CeO_2 nanoparticles effectively interacts with the surfactant-modified RGO nanosheet resulting in a facile electron channeling network, which in turn is responsible for the generation of the oxidation peak at 0.38 V [55].

Simultaneously, the fascinating redox property of CeO_2-anchored graphene nanohybrid also governs the electrocatalytic activity, which exhibits the removal of oxygen atoms from CeO_2 lattice unit generating two non-stoichiometric oxides CeO_2 and Ce_2O_3 that can reversibly

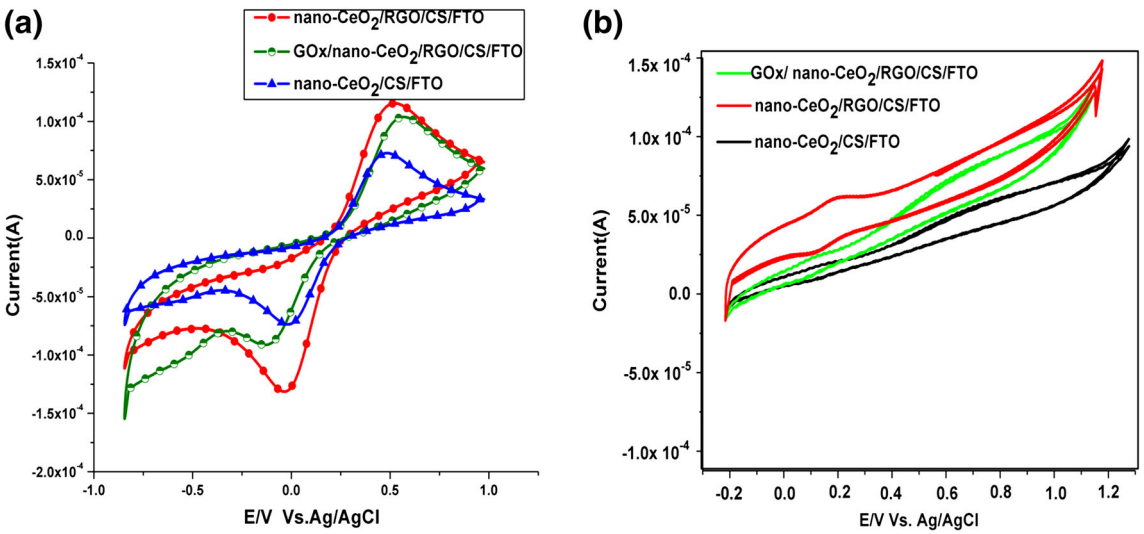

Fig. 9 Cyclic voltammetry studies of various modified electrodes in **a** 2.5 mM $[Fe(CN)_6]^{3-/4-}$ containing PBS buffer [pH 7.2, 0.1 (M) KCl], **b** blank media PBS buffer (pH 7.2) as control

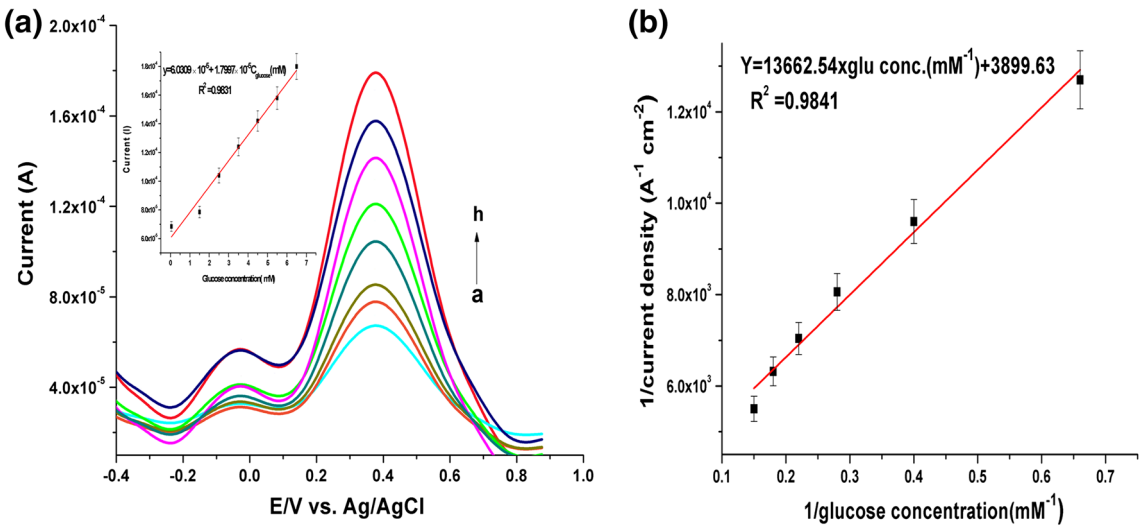

Fig. 10 **a** Typical amperometric differential pulse voltammetry curve of GOx/nano-CeO_2/RGO/CS/FTO bioelectrode with various glucose concentrations in air-saturated 0.1 (M) PBS buffer. The concentration of glucose **b** 0.05 mM, **c** 1.5 mM, **d** 2.5 mM, **e** 3.5 mM, **f** 4.5 mM, **g** 5.5 mM, **h** 6.5 mM. *Inset* is the corresponding calibration *curve*; **b** the calibrated Lineweaver–Burk plot for the bioelectrode

alter their oxidation state and exist as Ce^{4+}/Ce^{3+} redox couple under reducing condition [56]. In addition the evolution of H_2O_2 and its possible interaction with CeO_2 result in its reduction. Hence, an additional small peak appeared at ~ -0.03 V might be due to the oxidation of H_2O_2 molecule and its possible biochemical reaction was also represented in Scheme 2 [57].

As represented in the inset of Fig. 10a, the linear regression equation can be expressed as I (A) $= 6.0309 \times 10^{-5} + 1.7997 \times 10^{-5} \times C_{\text{glucose}}$ (mM) with a correlation coefficient of 0.983 (inset of Fig. 10). The increase in peak current response was observed after the addition of glucose analyte within the range of 0.05–6.5 mM. This could be ascribed to the electrocatalytic activity of the GOx/nano-CeO_2/RGO/CS/FTO-modified bioelectrode which assists in glucose monitoring. The oxygen consumption increased linearly with the increase in glucose concentration, indicating that with each successive addition of glucose analyte into O_2-saturated buffer which requires more oxygen for oxidation results in the linear enhancement of current responses [58].

Meanwhile the attained sensitivity of proposed bioelectrode has been estimated to be 7.198 μA mM^{-1} cm^{-2}, which is quite suitable and higher than the previously reported graphene-based biosensor for glucose detection (Table 1). The improved sensitivity was attributed to the fact that CeO_2-decorated RGO nanohybrid reinforced chitosan matrix provides enhanced electroactive surface which could facilitate the tunneling of electrons thus enhancing the sensitivity. Furthermore the secure distribution of CeO_2 nanoparticles on the RGO nanosheet renders large electroactive surface for the entrapment of enzyme biomolecules and efficiently accelerates the electron transfer reaction between the bioelectrode and the glucose analyte molecules leading to improved sensitivity in terms of current response [59]. Besides that, the preferable electrocatalytic property of the nano-CeO_2/RGO nanohybrid can be assigned due to the excellent synergistic coupling between redox-active CeO_2 NPs and highly conducting RGO nanosheet which induced the sensing performance of the bioelectrode as compared with other biosensor.

Scheme 2 The possible biochemical reaction pathway at GOx/nano-CeO_2/RGO/CS/FTO bioelectrode

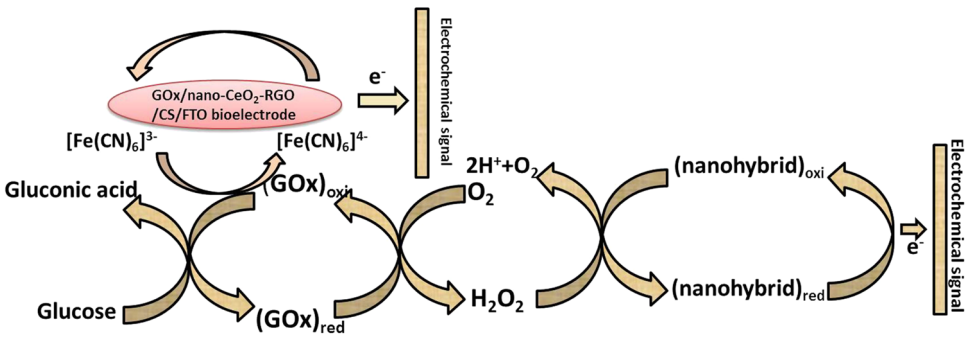

Table 1 Comparison of the electroanalytical parameters of the GOx/nano-CeO_2/RGO/CS/FTO bioelectrode with other GOx-based bioelectrodes

Electrode material	Linear range (mM)	Sensitivity (μA mM^{-1} cm^{-2})	References
PDDA GOx/Au/CNT[a]	0.5–5.0	2.5	[65]
GOx/Pt/FCNA/GCE[b]	0.5–8	6.0	[66]
Nafion/GOx/Ag/Pdop[c] @CNT/GCE	0.05–1.1	3.1	[67]
RGO/Ag/GOx	0.5–12.5	3.84	[68]
GOD/CeO_2 NRs	–	0.165	[69]
GOD-chitosan-BCNi	–	3.5	[70]
GOD/mesoporous TiO_2	–	3.9	[71]
GOD/porous carbon–silica	–	1.8	[72]
ERGO/CS/ZrO_2/GOD	0.2–1.6	7.6	[73]
SRGO/SmHCF/GCE[d]	50–250 μM	0.430	[55]
GOx/nano-CeO_2/RGO/CS/FTO	0.05–6.5	7.198	Present work

[a] Poly (diallyldimethylammonium chloride)

[b] Flower-like carbon nanosheet aggregation

[c] Polydopamine

[d] Samarium hexacyanoferrate

A response plateau in the calibration curve in Michaelis–Menten kinetic mechanism was employed to evaluate the enzyme substrate affinity (K_m^{app}) using Lineweaver–Burk plot given below:

$$1/I_{ss} = 1/I_{max} + K_m/I_{max}.C_{glucose},$$

where I_{SS} is the steady-state current response obtained after adding the substrate, C is the bulk concentration of the substrate, and I_{max} is the maximum current density observed under the saturated substrate concentration. The apparent Michaelis–Menten constant (K_m) was calculated from the slope of the calibration plot of steady-state current response ($1/I_{SS}$) versus analyte (glucose) concentration ($1/C_{glucose}$). As observed from the linear calibration curve (Fig. 10b), the maximum current density (I_{max}) was determined as 2.56×10^{-4} A^{-1} cm^{-2} from the intercept of the linear regression equation ($y = 13{,}662.54 \times$ glu conc. (mM^{-1}) + 3899.63, $R^2 = 0.9841$). Putting the value of I_{max} in the slope of above-mentioned equation, the K_m value was calculated and obtained as 3.5 mM implying that the GOx/nano-CeO_2/RGO/CS/FTO bioelectrode reveals higher electrocatalytic activity toward the determination of glucose. In addition, the lower value of K_m indicates that the fabricated chitosan nanocomposite matrix is highly suitable for effective enzyme immobilization as compared with other functionalized matrices [60, 61]. Moreover the low value of K_m (3.5 mM) also signifies the high enzymatic affinity and good biocompatibility of the GOx enzyme for its substrate glucose.

Additionally, the obtained linear detection range of the bioelectrode highlights the entire range of glucose concentrations found in the whole blood (3.5–5.3 mM), serum (2.5–5.3 mM), and urine (0.1–0.8 mM). The limit of detection (LOD) was also quantified to be 2 μM using the formula, LOD = 3SD/S, where S_D is the standard deviation of ten blank measurements and S is the sensitivity [62] ($S/N = 3$). This can also be associated with pH-responsive behavior of the bioelectrode. The response time of the bioelectrode has been estimated to be about 10 s, which shows rapid electron transportation across the nano-CeO_2/RGO/CS/FTO electrode.

Storage stability of the bioelectrode

The storage stability and shelf life of GOx/nano-CeO_2/RGO/CS/FTO bioelectrode was measured after an interval of 1 week and it has been continued to an additional 10 weeks. It was noted that the bioelectrode retained about 80.2 % of the entrapped GOx enzyme bioactivity even after 5 weeks when it was properly conditioned at 4 °C in a controlled and dry environment, whereas the magnitude of current response significantly decreased to 70.2 % in about 10 weeks. However, after 30 days of storage period the biosensor maintained ~89.5 % of its initial current response, which was much better than the earlier report [63]. These results reflect that the proposed biosensor had good long-term storage stability without any significant drift.

Selectivity in terms of interference study

For purpose of evaluating the selectivity of the biosensor, the impact of interferences on the response of GOx/nano-CeO_2/RGO/CS/FTO bioelectrode has been performed using cyclic voltammetry technique in a freshly prepared PBS [50 mM, pH 7.2] with 0.1 (M) KCl as a supporting electrolyte (Fig. 11). The selectivity of the bioelectrode has been monitored at their physiological concentrations such as urea (1 mM), lactic acid (LA) (1 mM), cholesterol (5 mM),

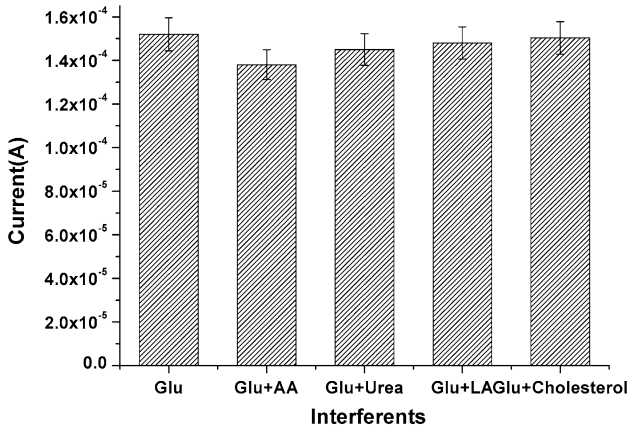

Fig. 11 Effect of interferents on GOx/nano-CeO_2/RGO/CS/FTO bioelectrode for glucose detection

ascorbic acid (AA) (0.05 mM), and glucose (Glu) (5 mM). The discrepancy in the magnitude of current response was examined in PBS buffer by injecting required amount of interfering substance in equal proportion with that of glucose analyte. Hence, it has been observed that the peak current density of the constructed bioelectrode was not remarkably influenced by the interferents implying no variation in peak current response. However, only ascorbic acid, lactic acid, and urea showed marginally reduced current value. The value of current response decreases by about 14, 7, and 4 % upon the addition of AA, urea, and LA, respectively which confirms that the bioelectrode is highly selective. These phenomena are in good accordance with the previous report [63, 64].

Conclusion

In summary, we have proposed the construction of a green biocompatible transducer platform based on nano-CeO_2/RGO nanohybrid reinforced chitosan nanocomposites electrode material for glucose monitoring. The resulting bioelectrode nano-CeO_2/RGO/CS/FTO provides a suitable microenvironment for effective immobilization of GOx enzyme and exhibits improved electrocatalytic activity toward glucose detection. The synergistic effect of CeO_2 NPs and RGO nanosheet may promote the electrochemical performance of fabricated bioelectrode which in turn leads to high sensitivity, wide detection range, and low detection limit efficient for glucose assessment. Furthermore, the composed nano-CeO_2/RGO nanohybrid-based chitosan nanocomposites was exploited as a promising biosensing platform in terms of biocompatibility, electrocatalytic sensitivity, and response time for the determination of glucose, which could also be extended in future to the miniaturization of MEMS and ISFT-based biosensors blending with micro-electronic technology for real-time monitoring process in the diagnostic area.

Acknowledgments One of the author Miss Sriparna De thanks Mrs. Lakshmi Unnikrishnan and Mr. K. Prabakaran from LARPM, CIPET for the support of the electrochemical characterization. This research received no specific grant from any funding agency in the public, commercial, or not-for-profit sectors.

References

1. Qureshia Anjum, Gurbuzb Yasar, Niazia Javed H (2012) Sensors Actuators B 171:62–76
2. Aronson D (2008) Hyperglycemia and the pathobiology of diabetic complications. In: Cardiovascular diabetology: clinical, metabolic and inflammatory facets; Fisman FX, Tenenbaum A, Eds; Karger: Basel, Swizerland, pp 1–16
3. Wild SR, Green A, Sicree R (2004) Diabetes Care 27:1047–1053
4. Eliane PC, María JAS, Manuela K, Vivian F (2014) J Mol Catal B Enzym 99:56–67
5. Teles FRR, Fonseca LP (2008) Mater Sci Eng C 28:1530–1543
6. Wu X, Sprinkle M, Li X, Ming F, Berger C, Heer WAD (2008) Phys Rev Lett 101:026801
7. Yoo JJ, Balakrishnan K, Huang J, Meunier V, Sumpter BG, Srivastava A, Conway M, Reddy ALM, Yu J, Vajtai R, Ajayan PM (2011) Nano Lett 11:1423–1427
8. Yang S, Cui G, Pang S, Cao Q, Kolb U, Feng X, Maier J, Mullen K (2010) Chem Sus Chem 3:236–239
9. Guo CX, Zhang LY, Miao J, Zhang J, Li CM (2013) Adv Energy Mater 3:167–171
10. Mani V, Periasamy AP, Chen SM (2012) Electrochem Commun 17:75–78
11. Mani V, Devadas B, Chen SM (2013) Biosens Bioelectron 41:309–315
12. Park S, Ruoff RS (2009) Nat Nanotechnol 4:217–244
13. Matsumoto Y, Koinuma M, Kim SY, Watanabe Y, Taniguchi T, Hatakeyama K, Tateishi H, Ida S (2010) ACS Appl Mater Interfaces 2:3461–3466
14. Kamat PV (2010) J Phys Chem Lett 1:520–527
15. Bolotin KI, Sikes KJ, Jiang Z, Klima M, Fudenberg G (2008) J Hone. Solid State Commun 146:351–355
16. Liang YY, Li YG, Wang HL, Zhou JG, Wang J, Regier T (2011) Nat Mater 10:780–786
17. Wu ZS, Ren WC, Wang DW, Li F, Liu BL, Cheng HM (2010) ACS Nano 10:5835–5842
18. Zhu Y, James DK, Tour JM (2012) Adv Mater 24:4924–4955
19. Cote LJ, Kim F, Huang JX (2009) Am Chem Soc J 131:1043–1049
20. Srivastava M, Das AK, Khanra P, Uddin MdE, Kima NH, Lee JH (2013) Mater Chem A J 1:9792–9801
21. De S, Mohanty S, Nayak SK (2014) J Mater Eng Perform 24(1):114–127
22. Du J, Lai XY, Yang NL, Zhai J, Kisailus D, Su FB, Wang D, Jiang L (2011) ACS Nano 5:590–596
23. De S, Mohanty S, Nayak SK (2015) Sens lett. doi:10.1166/s1.2015.3419
24. Wang ZL, Li GR, Ou YL, Feng ZP, Qu DL, Tong YX (2011) J Phys Chem C 115:351–356
25. Deluga GA, Salge JR, Schmidt LD, Verykios XE (2004) Science 303:993–997
26. Li D, Muller MB, Gilje S, Kaner RB, Wallace GG (2008) Nat Nanotechnol 3:101

27. Qiu JD, Huang J, Liang RP (2011) Sens Actuators B 160:287–294
28. Erdem A, Muti M, Karadeniz H, Congur G, Canavar E (2012) Colloids Surf B 95:222–228
29. Jiang L, Yao M, Liu B, Li Q, Liu R, Lv H, Lu S, Gong C, Zou B, Cui T, Liu B (2012) J Phys Chem C 116:11741–11745
30. Shan CS, Yang HF, Song JF, Han DX, Ivaska A, Niu L (2009) Anal Chem 81:2378–2382
31. Lu J, Do I, Drzal LT, Worden RM, Lee I (2008) ACS Nano 2:1825–1832
32. Lin WJ, Liao CS, Jhang JH, Tsai YC (2009) Electrochem Commun 11:2153–2156
33. Wu JF, Xu MQ, Zhao GC (2010) Electrochem Commun 12:175–177
34. Wang Y, Li Y, Tang L, Lu J, Li J (2009) Electrochem Commun 11:889–892
35. Li MX, Zhu JE, Zhang LL, Chen X, Zhang HM, Zhang FZ, Xu SL, Evans DG (2011) Nanoscale. doi:10.1039/C1NR10592B
36. Luo J, Jiang SS, Zhang HY, Jiang JQ, Liu X (2012) Anal Chim Acta 709:47–53
37. Lu LM, Li HB, Qu FL, Zhang XB, Shen GL, Yu RQ (2011) Biosens Bioelectron 26:3500–3504
38. Liu Y, Wang M, Zhao F, Xu Z, Dong S (2005) Biosens Bioelectron 21:984–988
39. Du D, Liu J, Zhang XY, Cui XL, Lin YH (2011) J Mater Chem 21:8032–8037
40. Wang G, Bai JT, Wang YH, Ren ZY, Bai JB (2011) Scr Mater 65:339–342
41. Amouzadeh M, Varkani TJN (2014) Sens Actuators B 202:475–482
42. Hummers WS, Offeman RE (1958) Am Chem Soc J 80:1339
43. Wang Y (2011) Guo CX, Liu JH, Chen T, Yang HB, Li CM. Dalton Trans 40:6388–6391
44. Jha SK, Kumar CN, Raj RP, Jha NS, Mohan S (2014) Electrochim Acta 120:308–313
45. Suh JKF, Matthew HWT (2000) Biomaterials 21:2589–2598
46. Dunn GA, Zicha D (1995) J Cell Sci 108:1239–1249
47. Muzzarelli C, Muzzarelli RAA (2002) J Inorg Biochem 92:89–94
48. Bose S, Darsell J, Hosick HL, Yang L, Sarkar DK, Bandyopadhyay A (2002) J Mater Sci Mater Med 13:23–28
49. Hannah S, Samuel SI (2005) Biomaterials 26:5492–5499
50. Costa HS, Mansur AAP, Barbosa-Stancioli EF, Pereira MM, Mansur HS (2008) J Mater Sci 43:510–524
51. Zhang M, Yuan R, Chai Y, Wang C, Wu X (2013) Anal Biochem 436:69–74
52. Suni II (2008) Trends Anal Chem 27:604–611
53. Maduraiveeran G, Ramaraj R (2007) J Electroanal Chem 608:52–58
54. Liu X, Xie L, Li H (2012) J Electroanal Chem 682:158–163
55. Devadas Balamurugan, Cheemalapati Srikanth, Chen Shen-Ming, Rajkumar Muniyandi (2014) RSC Adv 4:45895–45902
56. Chettibi S, Wojcieszak R, Boudjennad EH, Belloni J, Bettahar MM, Keghouche N (2006) Catal Today 113:157–165
57. Matharu Z, Sumanam G, Arya SK, Singh SP, Gupta V, Malhotra BD (2007) Langmuir 23(26):13188–13192
58. Kang Xinhuang, Jun Wang Hong Wu, Aksay Ilhan A, Liu Jun, Lin Yuehe (2009) Biosens Bioelectron 25:901–905
59. Teymourian Hazhir, Salimi Abdollah, Firoozi Somayeh, Korani Aazam (2014) Saied Soltanian Electrochimica Acta. doi:10.1016/j.electacta.2014.08.007
60. Zhao ZW, Chen XJ, Tay BK, Chen JS, Han ZJ, Khor KA (2007) Biosens Bioelectron 23:135–139
61. Wei Sun, Gao R, Jiao K (2007) J Phys Chem B 111:4560–4567
62. Radoi A, Compagnone D, Devic E, Palleschi G (2007) Sens Actuators B 121:501–506
63. Saha S, Arya SK, Singh SP, Sreenivas K, Malhotra BD, Gupta Vinay (2009) Biosens Bioelectron 24:2040–2045
64. Solanki PR, Dhand C, Kaushik A, Ansari AA, Sood KN, Malhotra BD (2009) Sens Actuators B 141:551–556
65. Ya YL, Shiu KK (2008) Electroanalysis 20:1542–1548
66. Tang S, Wang XZ, Lei JP, Hu Z, Deng SY, Ju HX (2010) Biosens Bioelectron 26:432–436
67. Wang YL, Liu L, Li MG, Xu SD, Gao F (2011) Biosens Bioelectron 30:107–111
68. Palanisamy S, Karuppiah C, Chen S (2014) Colloids Surf B 114:164–169
69. Patil D, Dung NQ, Jung H, Ahn SY, Jang DM, Kim D (2012) Biosens Bioelectron 31:176–181
70. Yang L, Xiong H, Zhang X, Wang S (2011) Biosens Bioelectron 26:3801–3805
71. Bao SJ, Li CM, Zang JF, Cui XQ, Qiao Y, Guo J (2008) Adv Funct Mater 18:591–599
72. Wu S, Ju H, Liu Y (2007) Adv Funct Mater 17:585–592
73. Cai Chang-Jun, Mao-Wen Xu, Bao Shu-Juan, Lei Chao, Jia Dian-Zeng (2012) RSC Adv 2:8172–8178